

Measurement of the integrated luminosity of the data collected at 3.773 GeV by BESIII from 2021 to 2024^{*}

M. Ablikim¹, M. N. Achasov^{4,c}, P. Adlarson⁷⁵, O. Afedulidis³, X. C. Ai⁸⁰, R. Aliberti³⁵, A. Amoroso^{74A,74C}, Q. An^{71,58,a}, Y. Bai⁵⁷, O. Bakina³⁶, I. Balossino^{29A}, Y. Ban^{46,h}, H.-R. Bao⁶³, V. Batozskaya^{1,44}, K. Begzsuren³², N. Berger³⁵, M. Berlowski⁴⁴, M. Bertani^{28A}, D. Betttoni^{29A}, F. Bianchi^{74A,74C}, E. Bianco^{74A,74C}, A. Bortone^{74A,74C}, I. Boyko³⁶, R. A. Briere⁵, A. Brueggemann⁶⁸, H. Cai⁷⁶, X. Cai^{1,58}, A. Calcaterra^{28A}, G. F. Cao^{1,63}, N. Cao^{1,63}, S. A. Cetin^{62A}, J. F. Chang^{1,58}, G. R. Che⁴³, G. Chelkov^{36,b}, C. Chen⁴³, C. H. Chen⁹, Chao Chen⁵⁵, G. Chen¹, H. S. Chen^{1,63}, H. Y. Chen²⁰, M. L. Chen^{1,58,63}, S. J. Chen⁴², S. L. Chen⁴⁵, S. M. Chen⁶¹, T. Chen^{1,63}, X. R. Chen^{31,63}, X. T. Chen^{1,63}, Y. B. Chen^{1,58}, Y. Q. Chen³⁴, Z. J. Chen^{25,i}, Z. Y. Chen^{1,63}, S. K. Choi^{10A}, G. Cibinetto^{29A}, F. Cossio^{74C}, J. J. Cui⁵⁰, H. L. Dai^{1,58}, J. P. Dai⁷⁸, A. Dbeysi¹⁸, R. E. de Boer³, D. Dedovich³⁶, C. Q. Deng⁷², Z. Y. Deng¹, A. Denig³⁵, I. Denysenko³⁶, M. Destefanis^{74A,74C}, F. De Mori^{74A,74C}, B. Ding^{66,1}, X. X. Ding^{46,h}, Y. Ding³⁴, Y. Ding⁴⁰, J. Dong^{1,58}, L. Y. Dong^{1,63}, M. Y. Dong^{1,58,63}, X. Dong⁷⁶, M. C. Du¹, S. X. Du⁸⁰, Y. Y. Duan⁵⁵, Z. H. Duan⁴², P. Egorov^{36,b}, Y. H. Fan⁴⁵, J. Fang⁵⁹, J. Fang^{1,58}, S. S. Fang^{1,63}, W. X. Fang¹, Y. Fang¹, Y. Q. Fang^{1,58}, R. Farinelli^{29A}, L. Fava^{74B,74C}, F. Feldbauer³, G. Felici^{28A}, C. Q. Feng^{71,58}, J. H. Feng⁵⁹, Y. T. Feng^{71,58}, M. Fritsch³, C. D. Fu¹, J. L. Fu⁶³, Y. W. Fu^{1,63}, H. Gao⁶³, X. B. Gao⁴¹, Y. N. Gao^{46,h}, Yang Gao^{71,58}, S. Garbolino^{74C}, I. Garzia^{29A,29B}, L. Ge⁸⁰, P. T. Ge⁷⁶, Z. W. Ge⁴², C. Geng⁵⁹, E. M. Gersabeck⁶⁷, A. Gilman⁶⁹, K. Goetzen¹³, L. Gong⁴⁰, W. X. Gong^{1,58}, W. Gradl³⁵, S. Gramigna^{29A,29B}, M. Greco^{74A,74C}, M. H. Gu^{1,58}, Y. T. Gu¹⁵, C. Y. Guan^{1,63}, A. Q. Guo^{31,63}, L. B. Guo⁴¹, M. J. Guo⁵⁰, R. P. Guo⁴⁹, Y. P. Guo^{12,g}, A. Guskov^{36,b}, J. Gutierrez²⁷, K. L. Han⁶³, T. T. Han¹, F. Hanisch³, X. Q. Hao¹⁹, F. A. Harris⁶⁵, K. K. He⁵⁵, K. L. He^{1,63}, F. H. Heinsius³, C. H. Heinz³⁵, Y. K. Heng^{1,58,63}, C. Herold⁶⁰, T. Holtmann³, P. C. Hong³⁴, G. Y. Hou^{1,63}, X. T. Hou^{1,63}, Y. R. Hou⁶³, Z. L. Hou¹, B. Y. Hu⁵⁹, H. M. Hu^{1,63}, J. F. Hu^{56,j}, S. L. Hu^{12,g}, T. Hu^{1,58,63}, Y. Hu¹, G. S. Huang^{71,58}, K. X. Huang⁵⁹, L. Q. Huang^{31,63}, X. T. Huang⁵⁰, Y. P. Huang¹, Y. S. Huang⁵⁹, T. Hussain⁷³, F. Hölzken³, N. Hüskens³⁵, N. in der Wiesche⁶⁸, J. Jackson²⁷, S. Janchiv³², J. H. Jeong^{10A}, Q. Ji¹, Q. P. Ji¹⁹, W. Ji^{1,63}, X. B. Ji^{1,63}, X. L. Ji^{1,58}, Y. Y. Ji⁵⁰, X. Q. Jia⁵⁰, Z. K. Jia^{71,58}, D. Jiang^{1,63}, H. B. Jiang⁷⁶, P. C. Jiang^{46,h}, S. S. Jiang³⁹, T. J. Jiang¹⁶, X. S. Jiang^{1,58,63}, Y. Jiang⁶³, J. B. Jiao⁵⁰, J. K. Jiao³⁴, Z. Jiao²³, S. Jin⁴², Y. Jin⁶⁶, M. Q. Jing^{1,63}, X. M. Jing⁶³, T. Johansson⁷⁵, S. Kabana³³, N. Kalantar-Nayestanaki⁶⁴, X. L. Kang⁹, X. S. Kang⁴⁰, M. Kavatsyuk⁶⁴, B. C. Ke⁸⁰, V. Khachatryan²⁷, A. Khoukaz⁶⁸, R. Kiuchi¹, O. B. Kolcu^{62A}, B. Kopf³, M. Kuessner³, X. Kui^{1,63}, N. Kumar²⁶, A. Kupsc^{44,75}, W. Kühn³⁷, J. J. Lane⁶⁷, L. Lavezzi^{74A,74C}, T. T. Lei^{71,58}, Z. H. Lei^{71,58}, M. Lellmann³⁵, T. Lenz³⁵, C. Li⁴⁷, C. Li⁴³, C. H. Li³⁹, Cheng Li^{71,58}, D. M. Li⁸⁰, F. Li^{1,58}, G. Li¹, H. B. Li^{1,63}, H. J. Li¹⁹, H. N. Li^{56,j}, Hui Li⁴³, J. R. Li⁶¹, J. S. Li⁵⁹, K. Li¹, L. J. Li^{1,63}, L. K. Li¹, Lei Li⁴⁸, M. H. Li⁴³, P. R. Li^{38,k,l}, Q. M. Li^{1,63}, Q. X. Li⁵⁰, R. Li^{17,31}, S. X. Li¹², T. Li⁵⁰, W. D. Li^{1,63}, W. G. Li^{1,a}, X. Li^{1,63}, X. H. Li^{71,58}, X. L. Li⁵⁰, X. Y. Li^{1,63}, X. Z. Li⁵⁹, Y. G. Li^{46,h}, Z. J. Li⁵⁹,

Received xxxx Month xxxx

* The BESIII Collaboration thanks the staff of BEPCII and the IHEP computing center for their strong support. This work is supported in part by National Key R&D Program of China under Contracts Nos. 2020YFA0406400, 2020YFA0406300, 2023YFA1606000; National Natural Science Foundation of China (NSFC) under Contracts Nos. 12035009, 11635010, 11735014, 11875054, 11935015, 11935016, 11935018, 11961141012, 12025502, 12035013, 12061131003, 12192260, 12192261, 12192262, 12192263, 12192264, 12192265, 12221005, 12225509, 12235017, 12361141819; the Chinese Academy of Sciences (CAS) Large-Scale Scientific Facility Program; the CAS Center for Excellence in Particle Physics (CCEPP); Joint Large-Scale Scientific Facility Funds of the NSFC and CAS under Contract Nos. U2032104, U1832207; the Excellent Youth Foundation of Henan Scientific Committee under Contract No. 242300421044; 100 Talents Program of CAS; The Institute of Nuclear and Particle Physics (INPAC) and Shanghai Key Laboratory for Particle Physics and Cosmology; German Research Foundation DFG under Contracts Nos. 455635585, FOR5327, GRK 2149; Istituto Nazionale di Fisica Nucleare, Italy; Ministry of Development of Turkey under Contract No. DPT2006K-120470; National Research Foundation of Korea under Contract No. NRF-2022R1A2C1092335; National Science and Technology fund of Mongolia; National Science Research and Innovation Fund (NSRF) via the Program Management Unit for Human Resources & Institutional Development, Research and Innovation of Thailand under Contract No. B16F640076; Polish National Science Centre under Contract No. 2019/35/O/ST2/02907; The Swedish Research Council; U. S. Department of Energy under Contract No. DE-FG02-05ER41374.

- Z. Y. Li⁷⁸, C. Liang⁴², H. Liang^{1,63}, H. Liang^{71,58}, Y. F. Liang⁵⁴, Y. T. Liang^{31,63}, G. R. Liao¹⁴, Y. P. Liao^{1,63}, J. Libby²⁶, A. Limphirat⁶⁰, C. C. Lin⁵⁵, D. X. Lin^{31,63}, T. Lin¹, B. J. Liu¹, B. X. Liu⁷⁶, C. Liu³⁴, C. X. Liu¹, F. Liu¹, F. H. Liu⁵³, Feng Liu⁶, G. M. Liu^{56,j}, H. Liu^{38,k,l}, H. B. Liu¹⁵, H. H. Liu¹, H. M. Liu^{1,63}, Huihui Liu²¹, J. B. Liu^{71,58}, J. Y. Liu^{1,63}, K. Liu^{38,k,l}, K. Y. Liu⁴⁰, Ke Liu²², L. Liu^{71,58}, L. C. Liu⁴³, Lu Liu⁴³, M. H. Liu^{12,g}, P. L. Liu¹, Q. Liu⁶³, S. B. Liu^{71,58}, T. Liu^{12,g}, W. K. Liu⁴³, W. M. Liu^{71,58}, X. Liu^{38,k,l}, X. Liu³⁹, Y. Liu⁸⁰, Y. Liu^{38,k,l}, Y. B. Liu⁴³, Z. A. Liu^{1,58,63}, Z. D. Liu⁹, Z. Q. Liu⁵⁰, X. C. Lou^{1,58,63}, F. X. Lu⁵⁹, H. J. Lu²³, J. G. Lu^{1,58}, X. L. Lu¹, Y. Lu⁷, Y. P. Lu^{1,58}, Z. H. Lu^{1,63}, C. L. Luo⁴¹, J. R. Luo⁵⁹, M. X. Luo⁷⁹, T. Luo^{12,g}, X. L. Luo^{1,58}, X. R. Lyu⁶³, Y. F. Lyu⁴³, F. C. Ma⁴⁰, H. Ma⁷⁸, H. L. Ma¹, J. L. Ma^{1,63}, L. L. Ma⁵⁰, M. M. Ma^{1,63}, Q. M. Ma¹, R. Q. Ma^{1,63}, T. Ma^{71,58}, X. T. Ma^{1,63}, X. Y. Ma^{1,58}, Y. Ma^{46,h}, Y. M. Ma³¹, F. E. Maas¹⁸, M. Maggiora^{74A,74C}, S. Malde⁶⁹, Y. J. Mao^{46,h}, Z. P. Mao¹, S. Marcello^{74A,74C}, Z. X. Meng⁶⁶, J. G. Messchendorp^{13,64}, G. Mezzadri^{29A}, H. Miao^{1,63}, T. J. Min⁴², R. E. Mitchell²⁷, X. H. Mo^{1,58,63}, B. Moses²⁷, N. Yu. Muchnoi^{4,c}, J. Muskalla³⁵, Y. Nefedov³⁶, F. Nerling^{18,e}, L. S. Nie²⁰, I. B. Nikolaev^{4,c}, Z. Ning^{1,58}, S. Nisar^{11,m}, Q. L. Niu^{38,k,l}, W. D. Niu⁵⁵, Y. Niu⁵⁰, S. L. Olsen⁶³, Q. Ouyang^{1,58,63}, S. Pacetti^{28B,28C}, X. Pan⁵⁵, Y. Pan⁵⁷, A. Pathak³⁴, Y. P. Pei^{71,58}, M. Pelizaeus³, H. P. Peng^{71,58}, Y. Y. Peng^{38,k,l}, K. Peters^{13,e}, J. L. Ping⁴¹, R. G. Ping^{1,63}, S. Plura³⁵, V. Prasad³³, F. Z. Qi¹, H. Qi^{71,58}, H. R. Qi⁶¹, M. Qi⁴², T. Y. Qi^{12,g}, S. Qian^{1,58}, W. B. Qian⁶³, C. F. Qiao⁶³, X. K. Qiao⁸⁰, J. J. Qin⁷², L. Q. Qin¹⁴, L. Y. Qin^{71,58}, X. P. Qin^{12,g}, X. S. Qin⁵⁰, Z. H. Qin^{1,58}, J. F. Qiu¹, Z. H. Qu⁷², C. F. Redmer³⁵, K. J. Ren³⁹, A. Rivetti^{74C}, M. Roloff^{74C}, G. Rong^{1,63}, Ch. Rosner¹⁸, S. N. Ruan⁴³, N. Salone⁴⁴, A. Sarantsev^{36,d}, Y. Schelhaas³⁵, K. Schoenning⁷⁵, M. Scodeggio^{29A}, K. Y. Shan^{12,g}, W. Shan²⁴, X. Y. Shan^{71,58}, Z. J. Shang^{38,k,l}, J. F. Shangguan¹⁶, L. G. Shao^{1,63}, M. Shao^{71,58}, C. P. Shen^{12,g}, H. F. Shen^{1,8}, W. H. Shen⁶³, X. Y. Shen^{1,63}, B. A. Shi⁶³, H. Shi^{71,58}, H. C. Shi^{71,58}, J. L. Shi^{12,g}, J. Y. Shi¹, Q. Q. Shi⁵⁵, S. Y. Shi⁷², X. Shi^{1,58}, J. J. Song¹⁹, T. Z. Song⁵⁹, W. M. Song^{34,1}, Y. J. Song^{12,g}, Y. X. Song^{46,h,n}, S. Sosio^{74A,74C}, S. Spataro^{74A,74C}, F. Stieler³⁵, Y. J. Su⁶³, G. B. Sun⁷⁶, G. X. Sun¹, H. Sun⁶³, H. K. Sun¹, J. F. Sun¹⁹, K. Sun⁶¹, L. Sun⁷⁶, S. S. Sun^{1,63}, T. Sun^{51,f}, W. Y. Sun³⁴, Y. Sun⁹, Y. J. Sun^{71,58}, Y. Z. Sun¹, Z. Q. Sun^{1,63}, Z. T. Sun⁵⁰, C. J. Tang⁵⁴, G. Y. Tang¹, J. Tang⁵⁹, M. Tang^{71,58}, Y. A. Tang⁷⁶, L. Y. Tao⁷², Q. T. Tao^{25,i}, M. Tat⁶⁹, J. X. Teng^{71,58}, V. Thoren⁷⁵, W. H. Tian⁵⁹, Y. Tian^{31,63}, Z. F. Tian⁷⁶, I. Uman^{62B}, Y. Wan⁵⁵, S. J. Wang⁵⁰, B. Wang¹, B. L. Wang⁶³, Bo Wang^{71,58}, D. Y. Wang^{46,h}, F. Wang⁷², H. J. Wang^{38,k,l}, J. J. Wang⁷⁶, J. P. Wang⁵⁰, K. Wang^{1,58}, L. L. Wang¹, M. Wang⁵⁰, N. Y. Wang⁶³, S. Wang^{12,g}, S. Wang^{38,k,l}, T. Wang^{12,g}, T. J. Wang⁴³, W. Wang⁵⁹, W. Wang⁷², W. P. Wang^{35,71,o}, X. Wang^{46,h}, X. F. Wang^{38,k,l}, X. J. Wang³⁹, X. L. Wang^{12,g}, X. N. Wang¹, Y. Wang⁶¹, Y. D. Wang⁴⁵, Y. F. Wang^{1,58,63}, Y. L. Wang¹⁹, Y. N. Wang⁴⁵, Y. Q. Wang¹, Yaqian Wang¹⁷, Yi Wang⁶¹, Z. Wang^{1,58}, Z. L. Wang⁷², Z. Y. Wang^{1,63}, Ziyi Wang⁶³, D. H. Wei¹⁴, F. Weidner⁶⁸, S. P. Wen¹, Y. R. Wen³⁹, U. Wiedner³, G. Wilkinson⁶⁹, M. Wolke⁷⁵, L. Wollenberg³, C. Wu³⁹, J. F. Wu^{1,8}, L. H. Wu¹, L. J. Wu^{1,63}, X. Wu^{12,g}, X. H. Wu³⁴, Y. Wu^{71,58}, Y. H. Wu⁵⁵, Y. J. Wu³¹, Z. Wu^{1,58}, L. Xia^{71,58}, X. M. Xian³⁹, B. H. Xiang^{1,63}, T. Xiang^{46,h}, D. Xiao^{38,k,l}, G. Y. Xiao⁴², S. Y. Xiao¹, Y. L. Xiao^{12,g}, Z. J. Xiao⁴¹, C. Xie⁴², X. H. Xie^{46,h}, Y. Xie⁵⁰, Y. G. Xie^{1,58}, Y. H. Xie⁶, Z. P. Xie^{71,58}, T. Y. Xing^{1,63}, C. F. Xu^{1,63}, C. J. Xu⁵⁹, G. F. Xu¹, H. Y. Xu^{66,2,p}, M. Xu^{71,58}, Q. J. Xu¹⁶, Q. N. Xu³⁰, W. Xu¹, W. L. Xu⁶⁶, X. P. Xu⁵⁵, Y. C. Xu⁷⁷, Z. S. Xu⁶³, F. Yan^{12,g}, L. Yan^{12,g}, W. B. Yan^{71,58}, W. C. Yan⁸⁰, X. Q. Yan¹, H. J. Yang^{51,f}, H. L. Yang³⁴, H. X. Yang¹, T. Yang¹, Y. Yang^{12,g}, Y. F. Yang^{1,63}, Y. F. Yang⁴³, Y. X. Yang^{1,63}, Z. W. Yang^{38,k,l}, Z. P. Yao⁵⁰, M. Ye^{1,58}, M. H. Ye⁸, J. H. Yin¹, Z. Y. You⁵⁹, B. X. Yu^{1,58,63}, C. X. Yu⁴³, G. Yu^{1,63}, J. S. Yu^{25,i}, T. Yu⁷², X. D. Yu^{46,h}, Y. C. Yu⁸⁰, C. Z. Yuan^{1,63}, J. Yuan³⁴, J. Yuan⁴⁵, L. Yuan², S. C. Yuan^{1,63}, Y. Yuan^{1,63}, Z. Y. Yuan⁵⁹, C. X. Yue³⁹, A. A. Zafar⁷³, F. R. Zeng⁵⁰, S. H. Zeng⁷², X. Zeng^{12,g}, Y. Zeng^{25,i}, Y. J. Zeng⁵⁹, Y. J. Zeng^{1,63}, X. Y. Zhai³⁴, Y. C. Zhai⁵⁰, Y. H. Zhan⁵⁹, A. Q. Zhang^{1,63}, B. L. Zhang^{1,63}, B. X. Zhang¹, D. H. Zhang⁴³, G. Y. Zhang¹⁹, H. Zhang⁸⁰, H. Zhang^{71,58}, H. C. Zhang^{1,58,63}, H. H. Zhang³⁴, H. H. Zhang⁵⁹, H. Q. Zhang^{1,58,63}, H. R. Zhang^{71,58}, H. Y. Zhang^{1,58}, J. Zhang⁸⁰, J. Zhang⁵⁹, J. J. Zhang⁵², J. L. Zhang²⁰, J. Q. Zhang⁴¹, J. S. Zhang^{12,g}, J. W. Zhang^{1,58,63}, J. X. Zhang^{38,k,l}, J. Y. Zhang¹, J. Z. Zhang^{1,63}, Jianyu Zhang⁶³, L. M. Zhang⁶¹, Lei Zhang⁴², P. Zhang^{1,63}, Q. Y. Zhang³⁴, R. Y. Zhang^{38,k,l}, S. H. Zhang^{1,63}, Shulei Zhang^{25,i}, X. D. Zhang⁴⁵, X. M. Zhang¹, X. Y. Zhang⁵⁰, Y. Zhang⁷², Y. Zhang¹, Y. T. Zhang⁸⁰, Y. H. Zhang^{1,58}, Y. M. Zhang³⁹, Yan Zhang^{71,58}, Z. D. Zhang¹, Z. H. Zhang¹, Z. L. Zhang³⁴, Z. Y. Zhang⁷⁶, Z. Y. Zhang⁴³, Z. Z. Zhang⁴⁵, G. Zhao¹, J. Y. Zhao^{1,63}, J. Z. Zhao^{1,58}, L. Zhao¹, Lei Zhao^{71,58}, M. G. Zhao⁴³, N. Zhao⁷⁸, R. P. Zhao⁶³, S. J. Zhao⁸⁰, Y. B. Zhao^{1,58}, Y. X. Zhao^{31,63}, Z. G. Zhao^{71,58}, A. Zhemchugov^{36,b}, B. Zheng⁷², B. M. Zheng³⁴, J. P. Zheng^{1,58}, W. J. Zheng^{1,63}, Y. H. Zheng⁶³, B. Zhong⁴¹, X. Zhong⁵⁹, H.

Zhou⁵⁰, J. Y. Zhou³⁴, L. P. Zhou^{1,63}, S. Zhou⁶, X. Zhou⁷⁶, X. K. Zhou⁶, X. R. Zhou^{71,58}, X. Y. Zhou³⁹, Y. Z. Zhou^{12,g}, J. Zhu⁴³, K. Zhu¹, K. J. Zhu^{1,58,63}, K. S. Zhu^{12,g}, L. Zhu³⁴, L. X. Zhu⁶³, S. H. Zhu⁷⁰, T. J. Zhu^{12,g}, W. D. Zhu⁴¹, Y. C. Zhu^{71,58}, Z. A. Zhu^{1,63}, J. H. Zou¹, J. Zu^{71,58}

(BESIII Collaboration)

¹ Institute of High Energy Physics, Beijing 100049, People's Republic of China

² Beihang University, Beijing 100191, People's Republic of China

³ Bochum Ruhr-University, D-44780 Bochum, Germany

⁴ Budker Institute of Nuclear Physics SB RAS (BINP), Novosibirsk 630090, Russia

⁵ Carnegie Mellon University, Pittsburgh, Pennsylvania 15213, USA

⁶ Central China Normal University, Wuhan 430079, People's Republic of China

⁷ Central South University, Changsha 410083, People's Republic of China

⁸ China Center of Advanced Science and Technology, Beijing 100190, People's Republic of China

⁹ China University of Geosciences, Wuhan 430074, People's Republic of China

¹⁰ Chung-Ang University, Seoul, 06974, Republic of Korea

¹¹ COMSATS University Islamabad, Lahore Campus, Defence Road, Off Raiwind Road, 54000 Lahore, Pakistan

¹² Fudan University, Shanghai 200433, People's Republic of China

¹³ GSI Helmholtzcentre for Heavy Ion Research GmbH, D-64291 Darmstadt, Germany

¹⁴ Guangxi Normal University, Guilin 541004, People's Republic of China

¹⁵ Guangxi University, Nanning 530004, People's Republic of China

¹⁶ Hangzhou Normal University, Hangzhou 310036, People's Republic of China

¹⁷ Hebei University, Baoding 071002, People's Republic of China

¹⁸ Helmholtz Institute Mainz, Staudinger Weg 18, D-55099 Mainz, Germany

¹⁹ Henan Normal University, Xinxiang 453007, People's Republic of China

²⁰ Henan University, Kaifeng 475004, People's Republic of China

²¹ Henan University of Science and Technology, Luoyang 471003, People's Republic of China

²² Henan University of Technology, Zhengzhou 450001, People's Republic of China

²³ Huangshan College, Huangshan 245000, People's Republic of China

²⁴ Hunan Normal University, Changsha 410081, People's Republic of China

²⁵ Hunan University, Changsha 410082, People's Republic of China

²⁶ Indian Institute of Technology Madras, Chennai 600036, India

²⁷ Indiana University, Bloomington, Indiana 47405, USA

²⁸ INFN Laboratori Nazionali di Frascati , (A)INFN Laboratori Nazionali di Frascati, I-00044, Frascati, Italy;

(B)INFN Sezione di Perugia, I-06100, Perugia, Italy; (C)University of Perugia, I-06100, Perugia, Italy

²⁹ INFN Sezione di Ferrara, (A)INFN Sezione di Ferrara, I-44122, Ferrara, Italy; (B)University of Ferrara, I-44122, Ferrara, Italy

³⁰ Inner Mongolia University, Hohhot 010021, People's Republic of China

³¹ Institute of Modern Physics, Lanzhou 730000, People's Republic of China

³² Institute of Physics and Technology, Peace Avenue 54B, Ulaanbaatar 13330, Mongolia

³³ Instituto de Alta Investigación, Universidad de Tarapacá, Casilla 7D, Arica 1000000, Chile

³⁴ Jilin University, Changchun 130012, People's Republic of China

³⁵ Johannes Gutenberg University of Mainz, Johann-Joachim-Becher-Weg 45, D-55099 Mainz, Germany

³⁶ Joint Institute for Nuclear Research, 141980 Dubna, Moscow region, Russia

³⁷ Justus-Liebig-Universitaet Giessen, II. Physikalisches Institut, Heinrich-Buff-Ring 16, D-35392 Giessen, Germany

³⁸ Lanzhou University, Lanzhou 730000, People's Republic of China

³⁹ Liaoning Normal University, Dalian 116029, People's Republic of China

⁴⁰ Liaoning University, Shenyang 110036, People's Republic of China

⁴¹ Nanjing Normal University, Nanjing 210023, People's Republic of China

⁴² Nanjing University, Nanjing 210093, People's Republic of China

⁴³ Nankai University, Tianjin 300071, People's Republic of China

⁴⁴ National Centre for Nuclear Research, Warsaw 02-093, Poland

⁴⁵ North China Electric Power University, Beijing 102206, People's Republic of China

⁴⁶ Peking University, Beijing 100871, People's Republic of China

⁴⁷ Qufu Normal University, Qufu 273165, People's Republic of China

⁴⁸ Renmin University of China, Beijing 100872, People's Republic of China

⁴⁹ Shandong Normal University, Jinan 250014, People's Republic of China

⁵⁰ Shandong University, Jinan 250100, People's Republic of China

⁵¹ Shanghai Jiao Tong University, Shanghai 200240, People's Republic of China

⁵² Shanxi Normal University, Linfen 041004, People's Republic of China

⁵³ Shanxi University, Taiyuan 030006, People's Republic of China

⁵⁴ Sichuan University, Chengdu 610064, People's Republic of China

⁵⁵ Soochow University, Suzhou 215006, People's Republic of China

⁵⁶ South China Normal University, Guangzhou 510006, People's Republic of China

⁵⁷ Southeast University, Nanjing 211100, People's Republic of China

⁵⁸ State Key Laboratory of Particle Detection and Electronics, Beijing 100049, Hefei 230026, People's Republic of China

⁵⁹ Sun Yat-Sen University, Guangzhou 510275, People's Republic of China

⁶⁰ Suranaree University of Technology, University Avenue 111, Nakhon Ratchasima 30000, Thailand
⁶¹ Tsinghua University, Beijing 100084, People's Republic of China

⁶² Turkish Accelerator Center Particle Factory Group, (A)Istanbul University, 34010, Istanbul, Turkey;
(B)Near East University, Nicosia, North Cyprus, 99138, Mersin 10, Turkey

⁶³ University of Chinese Academy of Sciences, Beijing 100049, People's Republic of China

⁶⁴ University of Groningen, NL-9747 AA Groningen, The Netherlands

⁶⁵ University of Hawaii, Honolulu, Hawaii 96822, USA

⁶⁶ University of Jinan, Jinan 250022, People's Republic of China

⁶⁷ University of Manchester, Oxford Road, Manchester, M13 9PL, United Kingdom

⁶⁸ University of Muenster, Wilhelm-Klemm-Strasse 9, 48149 Muenster, Germany

⁶⁹ University of Oxford, Keble Road, Oxford OX13RH, United Kingdom

⁷⁰ University of Science and Technology Liaoning, Anshan 114051, People's Republic of China

⁷¹ University of Science and Technology of China, Hefei 230026, People's Republic of China

⁷² University of South China, Hengyang 421001, People's Republic of China

⁷³ University of the Punjab, Lahore-54590, Pakistan

⁷⁴ University of Turin and INFN, (A)University of Turin, I-10125, Turin, Italy; (B)University of Eastern Piedmont, I-15121, Alessandria, Italy; (C)INFN, I-10125, Turin, Italy

⁷⁵ Uppsala University, Box 516, SE-75120 Uppsala, Sweden

⁷⁶ Wuhan University, Wuhan 430072, People's Republic of China

⁷⁷ Yantai University, Yantai 264005, People's Republic of China

⁷⁸ Yunnan University, Kunming 650500, People's Republic of China

⁷⁹ Zhejiang University, Hangzhou 310027, People's Republic of China

⁸⁰ Zhengzhou University, Zhengzhou 450001, People's Republic of China

^a Deceased

^b Also at the Moscow Institute of Physics and Technology, Moscow 141700, Russia

^c Also at the Novosibirsk State University, Novosibirsk, 630090, Russia

^d Also at the NRC "Kurchatov Institute", PNPI, 188300, Gatchina, Russia

^e Also at Goethe University Frankfurt, 60323 Frankfurt am Main, Germany

^f Also at Key Laboratory for Particle Physics, Astrophysics and Cosmology, Ministry of Education; Shanghai Key Laboratory for Particle Physics and Cosmology; Institute of Nuclear and Particle Physics, Shanghai 200240, People's Republic of China

^g Also at Key Laboratory of Nuclear Physics and Ion-beam Application (MOE) and Institute of Modern Physics, Fudan University, Shanghai 200443, People's Republic of China

^h Also at State Key Laboratory of Nuclear Physics and Technology, Peking University, Beijing 100871,

People's Republic of China

ⁱ Also at School of Physics and Electronics, Hunan University, Changsha 410082, China

^j Also at Guangdong Provincial Key Laboratory of Nuclear Science, Institute of Quantum Matter, South China Normal University, Guangzhou 510006, China

^k Also at MOE Frontiers Science Center for Rare Isotopes, Lanzhou University, Lanzhou 730000, People's Republic of China

^l Also at Lanzhou Center for Theoretical Physics, Lanzhou University, Lanzhou 730000, People's Republic of China

^m Also at the Department of Mathematical Sciences, IBA, Karachi 75270, Pakistan

ⁿ Also at Ecole Polytechnique Federale de Lausanne (EPFL), CH-1015 Lausanne, Switzerland

^o Also at Helmholtz Institute Mainz, Staudinger Weg 18, D-55099 Mainz, Germany

^p Also at School of Physics, Beihang University, Beijing 100191, China

Abstract We present a measurement of the integrated luminosity of e^+e^- collision data collected with the BESIII detector at the BEPCII collider at a center-of-mass energy of $E_{\text{cm}} = 3.773$ GeV. The integrated luminosities of the data sets taken from December 2021 to June 2022, from November 2022 to June 2023, and from October 2023 to February 2024 are determined to be (4.995 ± 0.019) fb^{-1} , (8.157 ± 0.031) fb^{-1} , and (4.191 ± 0.016) fb^{-1} , respectively, by analyzing large angle Bhabha scattering events. The uncertainties are dominated by systematic effects and the statistical uncertainties are negligible. Our results provide essential input for future analyses and precision measurements.

Key words Bhabha scattering events, integrated luminosity, cross section

1 Introduction

Luminosity plays a crucial role in quantifying the size of a dataset and is a fundamental parameter for measuring various physics processes, particularly cross sections. The number of events for the process $e^+e^- \rightarrow X$ (X denotes any possible final state) in e^+e^- collision data can be expressed as

$$N_{e^+e^- \rightarrow X} = \mathcal{L} \times \sigma_{e^+e^- \rightarrow X}(E_{\text{cm}}), \quad (1)$$

where \mathcal{L} denotes the integrated luminosity of the data set, $\sigma_{e^+e^- \rightarrow X}$ is the cross section for the process $e^+e^- \rightarrow X$, and E_{cm} is the center-of-mass energy. In principle, any process with a known cross section can be used to determine luminosity. However, Quantum Electrodynamics (QED) processes are advantageous due to their high production rates, simple final state topologies, and cross sections known with high theoretical precision.

Datasets at $E_{\text{cm}} = 3.773$ GeV were collected by the BESIII detector at the BEPCII collider from December 2021 to June 2022 (DATA I), from November 2022 to June 2023 (DATA II), and from October 2023 to February 2024 (DATA III) in order to systematically investigate the properties of $\psi(3770)$ and D meson production and decays. Precisely determining the luminosity of this dataset is important for various purposes. It is essential for measuring the cross section of $e^+e^- \rightarrow \psi(3770) \rightarrow D\bar{D}$, calculating the normalization factors in strong-

phase measurements of D^0 decays [1, 2], and reducing the systematic uncertainty of analyses using the single tag method. Additionally, the luminosity is used to normalize the Monte Carlo (MC) sample size and to estimate continuous background in the $\psi(3686)$ dataset. This paper presents a measurement of the integrated luminosity in DATA I, DATA II, and DATA III using large angle Bhabha scattering events. This dataset is currently the largest collection of e^+e^- collision data at the $\psi(3770)$ resonance peak in the world.

2 BESIII detector and Monte Carlo simulation

The BESIII detector [3] records symmetric e^+e^- collisions provided by the BEPCII storage ring [4] in the center-of-mass energy range from 2.0 to 4.95 GeV, with a peak luminosity of $1.1 \times 10^{33} \text{ cm}^{-2}\text{s}^{-1}$ achieved at $E_{\text{cm}} = 3.773$ GeV in 2023. BESIII has collected large data samples in this energy region [5–7]. The cylindrical core of the BESIII detector covers 93% of the full solid angle and consists of a helium-based multilayer drift chamber (MDC), a plastic scintillator time-of-flight system (TOF), and a CsI(Tl) electromagnetic calorimeter (EMC), which are all enclosed in a superconducting solenoidal magnet providing a 1.0 T magnetic field. The solenoid is supported by an octagonal flux-return yoke with resistive plate counter muon identification modules inter-

leaved with steel. The charged-particle momentum resolution at 1 GeV/c is 0.5%, and the dE/dx resolution is 6% for electrons from Bhabha scattering. The EMC measures photon energies with a resolution of 2.5% (5%) at 1 GeV in the barrel (end cap) region. The time resolution in the TOF barrel region is 68 ps, while that in the end cap region is 60 ps [8].

Simulated data samples produced with a GEANT4-based [9] Monte Carlo (MC) package, which includes the geometric description of the BESIII detector and the detector response, are used to determine detection efficiencies and to estimate backgrounds. The simulation models the beam energy spread and initial state radiation (ISR) in the e^+e^- annihilations with the generator KKMC [10]. The inclusive MC sample includes the production of $D\bar{D}$ pairs (including quantum coherence for the neutral D channels), the non- $D\bar{D}$ decays of the $\psi(3770)$, the ISR production of the J/ψ and $\psi(3686)$ states, and the continuum processes incorporated in KKMC [10].

All particle decays are modelled with EVTGEN [11] using branching fractions either taken from the Particle Data Group [12], when available, or otherwise estimated with LUNDCHARM [13]. Final state radiation (FSR) from charged final state particles is incorporated using the PHOTOS package [14].

The Bhabha signal events ($e^+e^- \rightarrow (\gamma)e^+e^-$) are simulated with the Babayaga@NLO generator [15–18]. The configuration parameters for the Babayaga@NLO generator are listed in Table 1. To account for beam energy fluctuations during data taking, a run-by-run calibration of E_{cm} has been performed and the calibrated E_{cm} is used as the center-of-mass energy in the generator. The duration of each run is typically one hour. The calibration of E_{cm} , which takes advantage of the small uncertainty in the known D mass m_D [12] and the excellent resolution of the MDC and EMC, is carried out using the following equations:

$$E_{cm} = 2E_D, E_D^2 = E_0^2 + (m_D c^2)^2 - (M_{BC}^{\text{fit}} c^2)^2. \quad (2)$$

Here, E_0 is the uncalibrated beam energy, i.e., 3.773 GeV, and M_{BC}^{fit} denotes the fitted peak of the beam-constrained mass of the D mesons. This is calculated using $M_{BC}^{\text{fit}} c^2 = \sqrt{E_0^2 - p_D^2 c^2}$, where p_D is the momentum of the D measured in the center-of-mass system of the e^+e^- collision using the decays $D^0 \rightarrow K^-\pi^+$, $D^0 \rightarrow K^-\pi^+\pi^+\pi^-$ and $D^+ \rightarrow K^-\pi^+\pi^+$. Essentially, Eq. 2 is equivalent to $E_D^2 = p^2 c^2 + m_D^2 c^4$.

The distributions of M_{BC} , instead of p_D , are utilized because M_{BC} offers better resolution and the fit to M_{BC} is more easily controlled. According to the above analysis, the calibrated E_{cm} varies by 2–3 MeV around the expected 3.773 GeV with an uncertainty of approximately 0.02 MeV. Details of the fit and particle reconstruction are introduced in Ref. [19].

Table 1: Configuration of the Babayaga@NLO generator used to simulate Bhabha events.

Parameter	Value
Center-of-mass energy	Calibrated E_{cm}
Beam Energy Spread	0.97 MeV
Minimum $\cos\theta$	-0.83
Maximum $\cos\theta$	0.83

3 Method

The integrated luminosity of data is usually measured with three QED processes: $e^+e^- \rightarrow (\gamma)e^+e^-$, $e^+e^- \rightarrow (\gamma)\gamma\gamma$ and $e^+e^- \rightarrow (\gamma)\mu^+\mu^-$. * However, the uncertainties associated with reconstructing γ and $\mu^{+(-)}$ particles are larger than those of $e^{+(-)}$. Moreover, Bhabha events at small angles, i.e., in the direction of the e^+e^- beam, predominantly interact with the end cap region of the detector. This region exhibits more gaps and lower resolution compared to the barrel region. The simulation at small angles is also less precise. Given that large angle Bhabha events provide negligible statistical uncertainty, we exclusively utilize them to measure the integrated luminosity of the data set. †

The integrated luminosity of data is determined by

$$\mathcal{L} = \sum_i \frac{N_i^{\text{obs}} \times (1 - \eta)}{\sigma_i \times \epsilon_i \times \epsilon^{\text{trig}}}. \quad (3)$$

In this equation, the index i indicates different runs and the integrated luminosity of the data set is obtained by summing over these runs. The variables N_i^{obs} , σ_i , ϵ_i , η , and ϵ^{trig} represents the number of observed Bhabha events, the production cross section of the Bhabha process, the detection efficiency, the contamination ratio, and the trigger efficiency for collecting events in the on-line data acquisition system, respectively. The Babayaga@NLO generator [15–18] is employed, using the E_{cm} calibrated on a run-by-run

*The symbol “(γ)” represents the possible presence of photon(s) resulting from ISR or FSR.

†The large angle region is defined as $|\cos\theta| < 0.83$, where θ is the polar angle of the final state electron (positron) relative to the beam direction.

basis, to calculate the cross section, generate signal MC events for the process $e^+e^- \rightarrow (\gamma)e^+e^-$, and estimate the detection efficiency.

4 Luminosity measurement

4.1 Event selection

Candidate Bhabha events are required to have exactly two oppositely charged tracks detected in the MDC. Each track is required to satisfy a distance of closest approach to the interaction point of less than 10 cm along the z axis (the symmetry axis of the MDC) and less than 1 cm in the transverse plane. Additionally, the candidate track must lie within the polar angle region $|\cos\theta| < 0.8$ to ensure interaction with the barrel of the EMC.

To suppress the $e^+e^- \rightarrow (\gamma)\mu^+\mu^-$ background, the deposited energy in the EMC (E_{EMC}), as shown in Fig. 1, must fall within the range of $1.0 < E_{\text{EMC}} < 2.5$ GeV. Furthermore, the sum of the momenta of the two tracks, as shown in Fig. 2, is required to be larger than $0.9 \times E_{\text{cm}}$ to suppress background events from processes involving a J/ψ in the final state, e.g., $e^+e^- \rightarrow (\gamma)J/\psi$, $e^+e^- \rightarrow (\gamma)\psi(3686) \rightarrow (\gamma)J/\psi X$, and $e^+e^- \rightarrow \psi(3770) \rightarrow (\gamma)J/\psi X$ ($J/\psi \rightarrow e^+e^-$ and $X = \pi^0\pi^0, \eta, \pi^0$ or $\gamma\gamma$). To further eliminate the background from energetic cosmic rays, the momenta of each track must be less than $E_{\text{cm}}/2 + 0.30$ GeV.

The two oppositely charged tracks in the candidate Bhabha scattering events are expected to be back-to-back. However, due to the presence of a magnetic field, their trajectories are bent, resulting in their respective shower clusters in the xy -plane of the EMC not being back-to-back. To quantify this angular difference, the variable $\delta\phi$ is defined as $|\phi_1 - \phi_2| - 180^\circ$, where ϕ_1 and ϕ_2 are the azimuthal angles of the two clusters in the EMC. The distribution of $\delta\phi$ is illustrated in Fig. 3 and a requirement of $5^\circ < |\delta\phi| < 40^\circ$ is imposed. This requirement effectively eliminates the background from the $e^+e^- \rightarrow (\gamma)\gamma\gamma$ process.

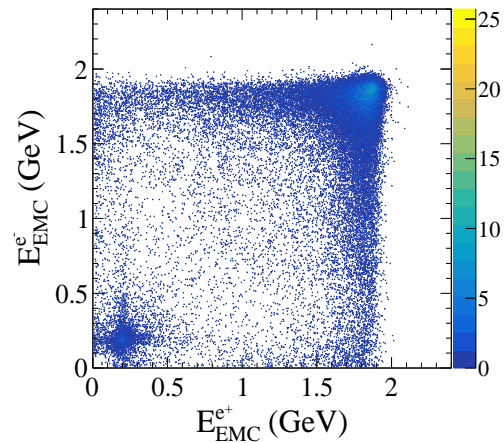


Figure 1: The distribution of $E_{\text{EMC}}^{e^+}$ versus $E_{\text{EMC}}^{e^-}$ from a subset of the data sample. The cluster concentrated at the upper right corner is the Bhabha signal and the small cluster at the lower left corner is the $e^+e^- \rightarrow (\gamma)\mu^+\mu^-$ background.

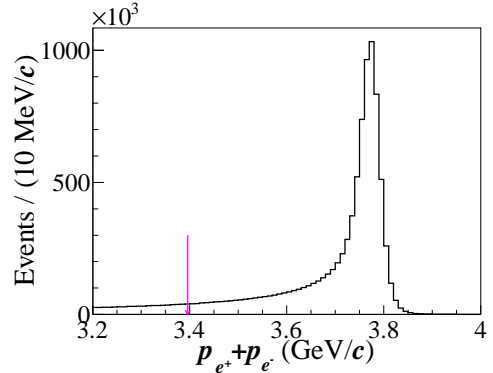


Figure 2: The distribution of $p_{e^+} + p_{e^-}$ from a subset of the data sample. The pink arrow indicates the $0.9 \times E_{\text{cm}}$ requirement.

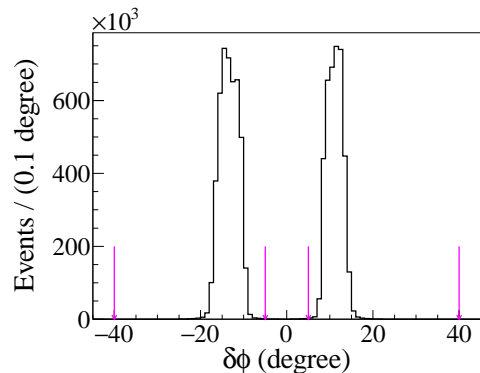


Figure 3: The distribution of $\delta\phi$ between the selected e^+ and e^- tracks from a subset of the data sample. The pink arrows indicate the $5^\circ < |\delta\phi| < 40^\circ$ requirement.

4.2 Background estimation

The residual background events are from various sources such as the ISR production of J/ψ and $\psi(3686)$, $e^+e^- \rightarrow (\gamma)\gamma\gamma$, $e^+e^- \rightarrow \psi(3770) \rightarrow D\bar{D}$, $e^+e^- \rightarrow \psi(3770) \rightarrow \text{non-}D\bar{D}$, and $e^+e^- \rightarrow$ continuum light hadron processes. These background contributions are estimated by analyzing background MC events, including $e^+e^- \rightarrow (\gamma)J/\psi$, $e^+e^- \rightarrow (\gamma)\psi(3686)$, $e^+e^- \rightarrow (\gamma)\gamma\gamma$, $e^+e^- \rightarrow (\gamma)\mu^+\mu^-$, $e^+e^- \rightarrow (\gamma)\tau^+\tau^-$, $e^+e^- \rightarrow \psi(3770) \rightarrow D^+D^-$, $e^+e^- \rightarrow \psi(3770) \rightarrow D^0\bar{D}^0$, $e^+e^- \rightarrow \psi(3770) \rightarrow \text{non-}D\bar{D}$, and $e^+e^- \rightarrow q\bar{q}$. The contamination rate for the candidate Bhabha events is calculated as $\eta = N_{\text{bkg}}^{\text{MC}} / (N_{\text{BB}}^{\text{MC}} + N_{\text{bkg}}^{\text{MC}})$, where $N_{\text{BB}}^{\text{MC}}$ and $N_{\text{bkg}}^{\text{MC}}$ are the numbers of Bhabha and background MC events that satisfy the selection criteria, respectively. These numbers are normalized according to individual cross sections. The resulting contamination rate is $\eta = 3 \times 10^{-4}$.

4.3 Detection efficiency and cross section

To estimate the detection efficiency for the Bhabha events, an $e^+e^- \rightarrow (\gamma)e^+e^-$ signal MC sample is generated for each run, using the calibrated E_{cm} , with the Babayaga@NLO generator [15–18]. The MC samples are generated within the range of $|\cos\theta| < 0.83$, where θ represents the polar angle of the final state e^+ and e^- . By applying the same selection criteria as used in the data analysis to these MC samples, the efficiency is calculated as the ratio of the number of selected signal MC events to the generated number of events. The cross section for each run is also estimated using Babayaga@NLO, taking into account the calibrated E_{cm} of each run. A total of 2 billion signal MC events are generated, which corresponds to approximately the same size as the data. This large sample size allows us to neglect the uncertainty arising from the statistics of the signal MC sample. The detection efficiency and cross section within $|\cos\theta| < 0.83$ at 3.773 GeV are determined to be 61.09% and 147.47 nb, respectively, with fluctuations on the order of 0.1% for different runs due to variations in E_{cm} .

4.4 Integrated luminosities

The number of observed Bhabha events for each run N_i^{obs} is determined by counting the events that satisfy the selection criteria outlined in Sec. 4.1. In total, 450.97×10^6 , 736.88×10^6 , and 379.45×10^6 events are obtained for DATA I, DATA II, and DATA III, respectively. The trigger efficiency ϵ^{trig} for collecting $e^+e^- \rightarrow (\gamma)e^+e^-$ events has been measured to

be 100% with a statistical uncertainty of less than 0.1% [20].

Inserting the number of observed Bhabha events, the trigger efficiency, the contamination rate (Sec. 4.2), the detection efficiency, and the cross sections within $|\cos\theta| < 0.83$ (Sec 4.3) into Eq. (3), the integrated luminosities are determined to be $(4.995 \pm 0.019) \text{ fb}^{-1}$ for DATA I, $(8.157 \pm 0.031) \text{ fb}^{-1}$ for DATA II, and $(4.191 \pm 0.016) \text{ fb}^{-1}$ for DATA III, where the statistical uncertainties are negligible and the systematic uncertainties will be discussed in the next subsection.

4.5 Systematic uncertainty

The systematic uncertainty arising from the MDC information, which includes the MDC tracking efficiency and the momentum requirement, is determined to be 0.29% by comparing the integrated luminosities measured with and without the MDC information. The systematic uncertainty associated with the E_{EMC} requirements is estimated by varying the requirement from 0.8 to 0.9 or 1.1 GeV. This variation results in a change of 0.16% in the luminosity for both tracks. To estimate the systematic uncertainty caused by the $\cos\theta$ requirement, the integrated luminosity is determined with $|\cos\theta| < 0.75$ or 0.70, and the difference from the standard selection of $|\cos\theta| < 0.80$ is found to be 0.13% for both tracks, which is assigned as the corresponding systematic uncertainty. The uncertainty due to the $\delta\phi$ signal region selection is estimated to be 0.02% by comparing the integrated luminosities obtained by changing the lower limit from 5° to 0° , or the higher limit from 40° to 20° or 30° . The uncertainty arising from the trigger efficiency [20] and the theoretically calculated cross section using the Babayaga@NLO generator [17] are both 0.1%. The uncertainties from the MC statistics and the contamination rate are negligible.

All contributions to the systematic uncertainty are summarized in Table 2. The total systematic uncertainty is obtained by adding all individual contributions in quadrature.

5 Summary

By analyzing large angle Bhabha scattering events, we have measured the integrated luminosity of the e^+e^- collision data collected at $E_{\text{cm}} = 3.773$ GeV from the years 2021 to 2024 with the BESIII detector at the BEPCII collider. These are crucial normalization factors for experimental studies of the production and decays of the $\psi(3770)$ and D mesons. Using

the cross sections of $\sigma(e^+e^- \rightarrow D^0\bar{D}^0) = (3.615 \pm 0.010_{\text{stat}} \pm 0.038_{\text{syst}})$ nb and $\sigma(e^+e^- \rightarrow D^+D^-) = (2.830 \pm 0.011_{\text{stat}} \pm 0.026_{\text{syst}})$ nb [21], one can obtain the numbers of $D^0\bar{D}^0$ and D^+D^- pairs in data. All the numerical results are summarized in Table 3. Along with the (2.932 ± 0.014) fb^{-1} data collected from 2010 to 2011 [22, 23], BESIII has accumulated data sets with a total integrated luminosity of (20.275 ± 0.077) fb^{-1} at $E_{\text{cm}} = 3.773$ GeV. These results offer fundamental inputs for physics analyses based on these data samples [24, 25].

Table 2: The relative systematic uncertainties in the luminosity determination.

Source	Uncertainty (%)
MDC information	0.29
E_{EMC}	0.16
$\cos\theta$	0.13
$\delta\phi$	0.02
Trigger	0.10
Generator	0.10
Total	0.38

References

- 1 M. Ablikim *et al.* (BESIII Collaboration), *Phys. Rev. Lett.* **124**, 241802 (2020).
- 2 M. Ablikim *et al.* (BESIII Collaboration), *Phys. Rev. D* **101**, 112002 (2020).
- 3 M. Ablikim *et al.* (BESIII Collaboration), *Nucl. Instrum. Meth. Phys. Res. Sect. A* **614**, 345 (2010).
- 4 C. H. Yu *et al.*, Proceedings of IPAC2016, Busan, Korea, 2016, doi:10.18429/JACoW-IPAC2016-TUYA01.
- 5 M. Ablikim *et al.* (BESIII Collaboration), *Chin. Phys. C* **44**, 040001 (2020).
- 6 J. Lu, Y. Xiao, and X. Ji, *Radiat. Detect. Technol. Methods* **4**, 337 (2020).
- 7 J. W. Zhang *et al.*, *Radiat. Detect. Technol. Methods* **6**, 289 (2022).
- 8 X. Li *et al.*, *Radiat. Detect. Technol. Methods* **1**, 13 (2017); Y. X. Guo *et al.*, *Radiat. Detect. Technol. Methods* **1**, 15 (2017); P. Cao *et al.*, *Nucl. Instrum. Meth. A* **953**, 163053 (2020).
- 9 S. Agostinelli *et al.* (GEANT4 Collaboration), *Nucl. Instrum. Meth. A* **506**, 250 (2003).
- 10 S. Jadach, B. F. L. Ward, and Z. Was, *Phys. Rev. D* **63**, 113009 (2001); *Comput. Phys. Commun.* **130**, 260 (2000).
- 11 D. J. Lange, *Nucl. Instrum. Meth. A* **462**, 152 (2001); R. G. Ping, *Chin. Phys. C* **32**, 599 (2008).
- 12 R. L. Workman *et al.* (Particle Data Group), *Prog. Theor. Exp. Phys.* **2022**, 083C01 (2022) and 2023 update.
- 13 J. C. Chen, G. S. Huang, X. R. Qi, D. H. Zhang, and Y. S. Zhu, *Phys. Rev. D* **62**, 034003 (2000); R. L. Yang, R. G. Ping and H. Chen, *Chin. Phys. Lett.* **31**, 061301 (2014).
- 14 E. Richter-Was, *Phys. Lett. B* **303**, 163 (1993).
- 15 C.M. Carloni Calame *et al.*, *Nucl. Phys. B Proc. Suppl.* **131**, 48 (2004).
- 16 G. Balossini *et al.*, *Nucl. Phys. B* **758**, 227 (2006).
- 17 G. Balossini *et al.*, *Phys. Lett. B* **663**, 209 (2008).
- 18 S. Actis *et al.*, *Eur. Phys. J. C* **66**, 585 (2010).
- 19 M. Ablikim *et al.* (BESIII Collaboration), *Chin. Phys. C* **46**, 113003 (2022).
- 20 N. Berger *et al.*, *Chin. Phys. C* **34**, 1779 (2010).
- 21 M. Ablikim *et al.* (BESIII Collaboration), *Chin. Phys. C* **42**, 083001 (2018).
- 22 M. Ablikim *et al.* (BESIII Collaboration), *Phys. Lett. B* **753**, 629 (2016).
- 23 M. Ablikim *et al.* (BESIII Collaboration), *Chin. Phys. C* **37**, 123001 (2013).
- 24 B. C. Ke, J. Koponen, H. B. Li and Y. Zheng, *Ann. Rev. Nucl. Part. Sci.* **73**, 285-314 (2023).
- 25 H. B. Li and X. R. Lyu, *Natl. Sci. Rev.* **8**, no.11, nwab181 (2021).

Table 3: Numerical results for DATA I, DATA II, and DATA III along with data collected from 2010 to 2011 (DATA 2010) [22], the number of observed events (N_{obs}), the integrated luminosity (\mathcal{L}), and the numbers of $D^0\bar{D}^0$ ($N_{D^0\bar{D}^0}$) and D^+D^- ($N_{D^+D^-}$).

Sample	$N_{\text{obs}} (10^6)$	$\mathcal{L} (\text{fb}^{-1})$	$N_{D^0\bar{D}^0} (10^6)$	$N_{D^+D^-} (10^6)$
DATA I	450.97	4.995 ± 0.019	18.06 ± 0.21	14.14 ± 0.16
DATA II	736.88	8.157 ± 0.031	29.49 ± 0.34	23.08 ± 0.25
DATA III	379.45	4.191 ± 0.016	15.15 ± 0.18	11.86 ± 0.13
DATA 2010 [22]	283.95	2.932 ± 0.014	10.60 ± 0.13	8.30 ± 0.09
TOTAL	1851.25	20.275 ± 0.077	73.29 ± 0.84	57.38 ± 0.61